JrnlID 11307_ArtID 141_Proof# 1 - 07/04/2008

MOLECULAR IMAGING AND BIOLOGY

Mol Imaging Biol (2008)
DOI: 10.1007/s11307-008-0141-8

RESEARCH ARTICLE

Animal PET for Thioacetamide-Induced Rat Cholangiocarcinoma

A Novel and Reliable Platform

Chun-Nan Yeh,[1] Kun-Ju Lin,[2,3] Ing-Tsung Hsiao,[2,3] Tzu-Chen Yen,[2] Tsung-Wen Chen,[1] Yi-Yin Jan,[1] Yi-Shiu Chung,[3] Chung-Fu Lin,[3] Miin-Fu Chen[1]

[1]*Department of Surgery, Chang Gung Memorial Hospital, Chang Gung University, 5, Fu-Hsing Street, Kwei-Shan, Taoyuan, Taiwan*
[2]*Department of Nuclear Medicine and Molecular Imaging Center, Chang Gung Memorial Hospital, Taoyuan, Taiwan*
[3]*Department of Medical Imaging and Radiological Sciences, Chang Gung University, Taoyuan, Taiwan*

Abstract

Purpose: Cholangiocarcinoma (CCA) is a lethal disease afflicting many thousands of patients worldwide. We have previously developed an oral thioacetamide (TAA)-induced model of rat CCA that recapitulates the histologic progression of human CCA. Our objective was to evaluate the feasibility of animal PET in detecting CCA in the setting of the TAA rat model.

Procedures: Male Sprague–Dawley rats (n=30) were used in this study. Drinking water with TAA 300 mg/l was administered orally in 26 rats, and animal PET was performed at 20 weeks after initiation of TAA. A total of four rats served as controls. Animal PET images were acquired sequentially using both C-11 acetate and 2-deoxy-2-[F-18]fluoro-D-glucose (FDG) to determine the optimal tracer. Dynamic animal PET images were collected to assess the optimal scan time based on the highest tumor-to-liver (T/L) ratio using time–activity curves. Animal PET findings were compared lesion by lesion with the results of autoradiography and the histological data.

Results: FDG animal PET images had a higher T/L ratio compared to images obtained with C-11 acetate as a marker. The optimal scan time for FDG animal PET was determined as 90 min postinjection of the tracer. This was when the T/L ratio reached its peak. Necropsy and histology confirmed the presence of TAA-induced CCA in 22 rats (84.6 %). Static animal PET images showed intense FDG uptake in 17 of the 22 tumor-bearing animals (77.3%). The average T/L ratio was 1.60±0.09. The sensitivity and specificity of animal PET in the detection of CCA were 77% (17/22) and 100% (4/4), respectively.

Conclusions: We conclude that animal PET in the setting of the TAA rat model seems to be feasible for the detection of CCA. Future translational studies are needed to confirm and expand our findings.

Key words: Animal PET, Cholangiocarcinoma, FDG, Thioacetamide

Introduction

Cholangiocarcinoma (CCA) is a lethal disease, afflicting approximately 3,000 individuals in the USA and many thousands more the world over. The mortality from intrahepatic CCAs is very high, with the 5-year survival rates being <15–20% in most series [1, 2]. There are numerous risk factors for CCA including primary sclerosing cholangitis, parasitic infections, choledochal cysts, hepatolithiasis, and carcinogen exposure [1, 3]. Increasing evidence suggests that human CCA proceeds through a multistep process and that invasive CCA is preceded by dysplasia in the biliary epithelium [4]. Recently, major progress has been made in understanding

C-N Yeh and K-J Lin contributed equally to this work.

Correspondence to: Miin-Fu Chen; *e-mail:* lin4857@adm.cgmh.org.tw

the molecular basis of CCA. Aberrant autocrine expression of hepatocyte growth factor/scatter factor is frequently detected in CCA and is likely contribute to oncogenesis in the biliary tract [7]. Other alterations that seem to occur early in cholangiocarcinogenesis include over-expression of the receptor tyrosine kinases (RTKs), ErbB-2, and Met [5–7].

Thus far, preclinical therapeutic investigations in CCA have been conducted *in vitro* [8] or in studies involving tumor xenografts [9]. Under these circumstances, preclinical animal models may be a major tool for the selection and development of anticancer agents for treating this malignancy [10]. We have previously developed an oral thioacetamide (TAA)-induced model of rat CCA that recapitulates the histologic progression of human CCA [11]. The TAA rat model may thus serve as a powerful preclinical platform for evaluating therapeutic strategies in invasive CCA.

In recent years, tumor response to therapeutics has been detected by a combination of direct tumor measurement and molecular imaging methods, including 2-deoxy-2-[F-18] fluoro-D-glucose (FDG)-positron emission tomography (PET) [12]. Notably, FDG-PET is useful in detecting the primary lesion in both hilar and peripheral CCA [13]. In addition, several recent studies have demonstrated that C-11 acetate may be a useful tracer for various cancer types [14, 15]. It is worth noting that C-11 acetate has a high sensitivity and specificity as a radiotracer complementary to FDG in the PET imaging of hepatocellular carcinoma [14, 16].

A very recent study has shown that the TAA rat model is a valuable experimental tool that, in combination with FDG PET, may allow the evaluation of pharmacological interventions in CCA [17].These findings prompted us to evaluate the feasibility of animal PET in detecting CCA in the setting of the TAA rat model. In the present study, animal PET images were acquired sequentially using both C-11 acetate and FDG to determine the optimal tracer. Animal PET findings were also compared lesion by lesion with the results of autoradiography and the histological data.

Materials and Methods

Animal Studies

The experimental animal ethics committee of Chang Gung Memorial Hospital approved all animal protocols in this study. Furthermore, the investigation conformed to the US National Institute of Health (NIH) guidelines for the care and use of laboratory animals (Publication No. 85–23, revised 1996). Thirty adult male Sprague–Dawley (SD) rats (weight=319±14 g, mean±SD) were used in these experiments. The animals were divided into two groups, including a control group (n=4) and an experiment group (n=26). The rats were housed in an animal room with a 12:12-h light–dark cycle (light from 0800 to 2000 hours) at an ambient temperature of 22±1°C, with food and water available ad libitum. The experiment group rats were administered 300 mg TAA/l in their drinking water every day up to 20 weeks. The control group rats were administered normal drinking water everyday up to 20 weeks. During the experiment, the animals were weighed weekly to calculate their body weight gain.

Animal PET

Image acquisition was performed on an Inveon™ system (Siemens Medical Solutions, USA, Inc.). The scanner has an axial field of view (FOV) of 12.7 cm and a transaxial FOV of 10.0 cm. One bed position is thus sufficient to cover the entire rat body area. Data were corrected for dead-time losses, random coincidences, and radioactive decay. The scanner has a peak system sensitivity of 6.8% at the center of the field of view (CFOV) and features high spatial resolution (1.4 mm FWHM).

Comparison of PET Radiotracers

C-11 acetate was prepared as described earlier [18]. FDG was produced according to the method described by Füchtner [19]. Animals fasted overnight under the standard condition of light and free access to water. Warming was started 30 minutes before radiotracer injection and continued throughout the uptake and imaging period under a tungsten lamp. The scanning room temperature was controlled at 24°C at all time. Under temporary isoflurane anesthesia, 2 mCi (74 MBq) of C-11 acetate was administered intravenously, and a dynamic frame acquisition was initiated simultaneously. The total acquisition time was 40 minutes. The scanning was started from the neck to ensure a whole coverage of the lung and liver in one bed position. The next day, 0.5 mCi (18.5 MBq) of FDG was administered intravenously under the same experimental conditions. The total acquisition time was 120 minutes. Volumes of interest (VOIs) were drawn around the tumor volume and the surrounding normal liver tissue. The tumor-to-liver (T/L) activity ratio was also calculated.

Determination of Optimal Scan Time

In a pilot experiment, serial dynamic scans were performed in six rats from the experiment group. The 2-hour list-mode image acquisition (2 minutes×5 frames, 5 minutes×4 frames, and 10 minutes×9 frames) was started immediately after radiotracer injection. To augment the anatomical data obtained from animal PET, microcomputed tomography (NanoSPECT/CT, Bioscan, USA) was performed immediately after the PET acquisition using the same scanning bed. Micro-CT data were acquired using high-resolution frames (55 keV tube voltage, 500 ms exposure time, 180 projections). Helical pitch was set to be of 2 to enable lung and liver scanning. CT data were reconstructed with the NanoSPECT/CT software using a "fine" reconstruction mode (512×512×480 voxels, 0.2 mm voxel size). PET and CT images were fused automatically for visual interpretation using the PMOD image analysis software (PMOD Technologies Ltd, Zurich, Switzerland; Fig. 1).

Regions of interest (ROIs) were drawn around the tumor volume and the surrounding normal liver tissue. Next, the time–activity curve and the T/L ratio were calculated. The optimal scan time for obtaining the maximal T/L ratio was determined. In all animals (n=6), static images were generated from dynamic images obtained at the optimal scan time for later interpretation.

Static Animal PET Imaging

Based on actual data obtained in the course of the pilot study, static animal PET studies were conducted in 24 rats from the experiment group. List mode image data were acquired and were rebinned into 2D sinograms using Fourier rebinning method. Images were reconstructed using 2D OSEM method (4 iterations and 16 subsets) without attenuation and scatter corrections. A total of 159 slices (x–y pixel size: 0.0861 cm, slice thickness: 0.0796 cm) with 128×128 matrix were acquired. To obtain a calibration factor relating animal PET measurement to the activity in the dose calibrator source, a cylindrical phantom (3.0 cm diameter) filled with FDG solution was scanned.

Necropsy and Ex Vivo Autoradiography

After static animal PET scans were completed, the rats were killed by overdose of pentobarbital (100 mg/kg intraperitoneally). Following a midline laparotomy, all lobes of the liver were explored and thoroughly examined. Harvesting procedure and histopathological evaluation of the liver was performed as previously described [11]. The uptake of radiotracer in the liver was assessed with autoradiography according to previous methodology [20]. Sections were cut at 40 μm thickness for autoradiography and at 10 μm for hematoxylin–eosin staining.

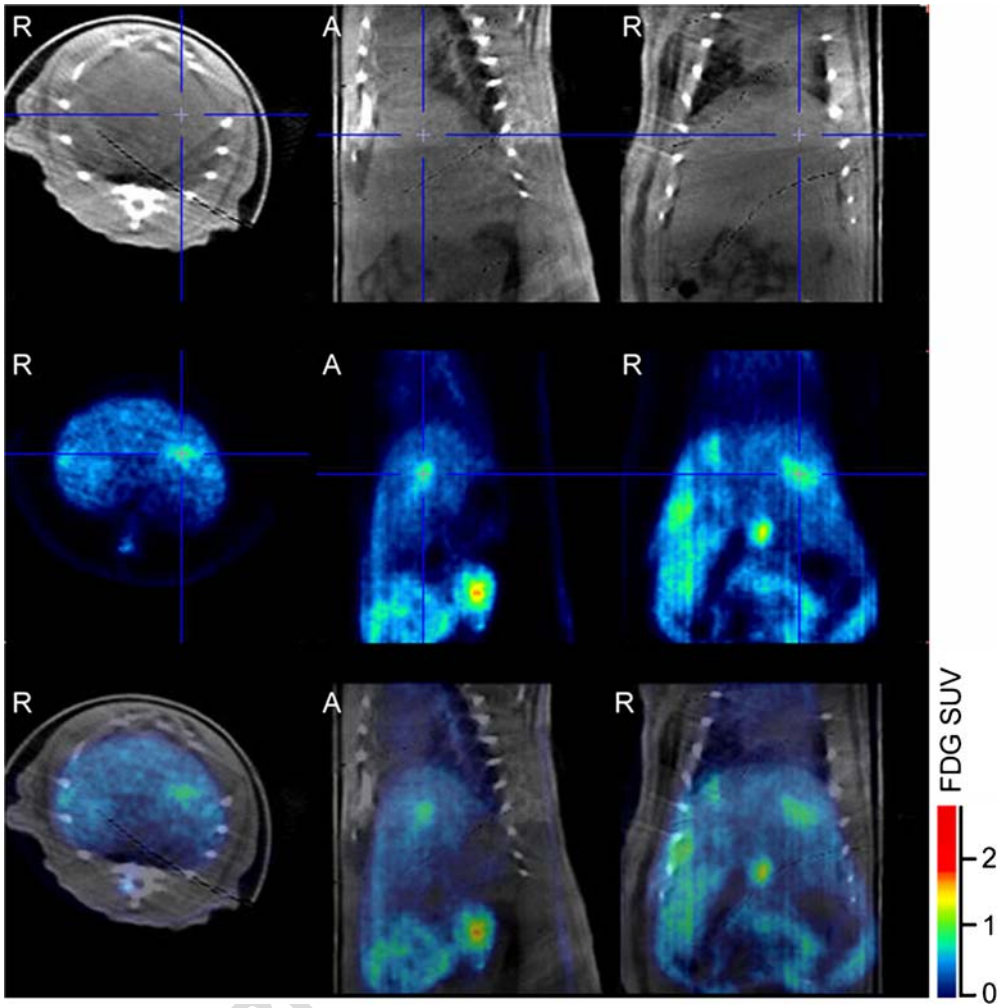

Fig. 1. Transverse, sagittal, and coronal views of CT and PET studies. CT and PET images were fused to improve interpretation accuracy (*third column*).

For autoradiographic studies, sections were rapidly dried in a stream of warm air and exposed to Fuji Storage Phosphor Image Plates (Phosphor Imager system, Fujifilm, Japan) for 24 hours. FDG uptake and the T/L ratio were measured from autoradiography.

Animal PET Image Analysis

Quantification of tracer uptake was performed by the calculation of the standardized uptake value (SUV) according to the following formula:

$$\mathrm{SUV} = \frac{\text{Decay corrected tissue activity (Bq/mL)}}{\text{Injected dose (Bq)/Body weight (g)}}$$

according to the European Organization for Research and Treatment of Cancer recommendations [21]. The maximum and mean SUV (SUV_{max} and SUV_{mean}) were calculated within the VOIs. FDG uptake was investigated in all animals. Animal PET findings were compared lesion by lesion with the results of autoradiography and the histological data.

Data Analysis

Data are presented as means±SDs, and differences between the study and control groups were determined using an independent two-sample Mann–Whitney *U* test and the Kruskal–Wallis test when appropriate. Data analysis was performed using SPSS computer software (Chicago, IL, USA), with a p value of <0.05 being considered statistically significant.

Results

Systemic Effects of TAA Administration

There were no instances of TAA-induced mortality during the 20-week study period. Significantly lower body weight gain was observed in the TAA-fed rats (452±35 g) compared with the control rats (567±12 g) at 20 weeks posttreatment.

Scan Protocol and Comparison of Radiotracers

In the pilot dynamic study, the maximal T/L ratio was 1.2± 0.2 for C-11 acetate and 1.8±0.2 for FDG. There was a higher T/L contrast for FDG versus C-11 acetate (Fig. 2). Thus, FDG was chosen for the following dynamic studies. The time–activity curves were characterized by a gradual decrease in the tumor volume and the surrounding normal liver tissue after tracer injection. There was a gradual increase in T/L ratio over time revealing a peak about 90 minutes after tracer injection (Fig. 3). Then, the ratio stabilized for 30 minutes and declined thereafter. In the light of these results, the optimal scan time for animal PET was

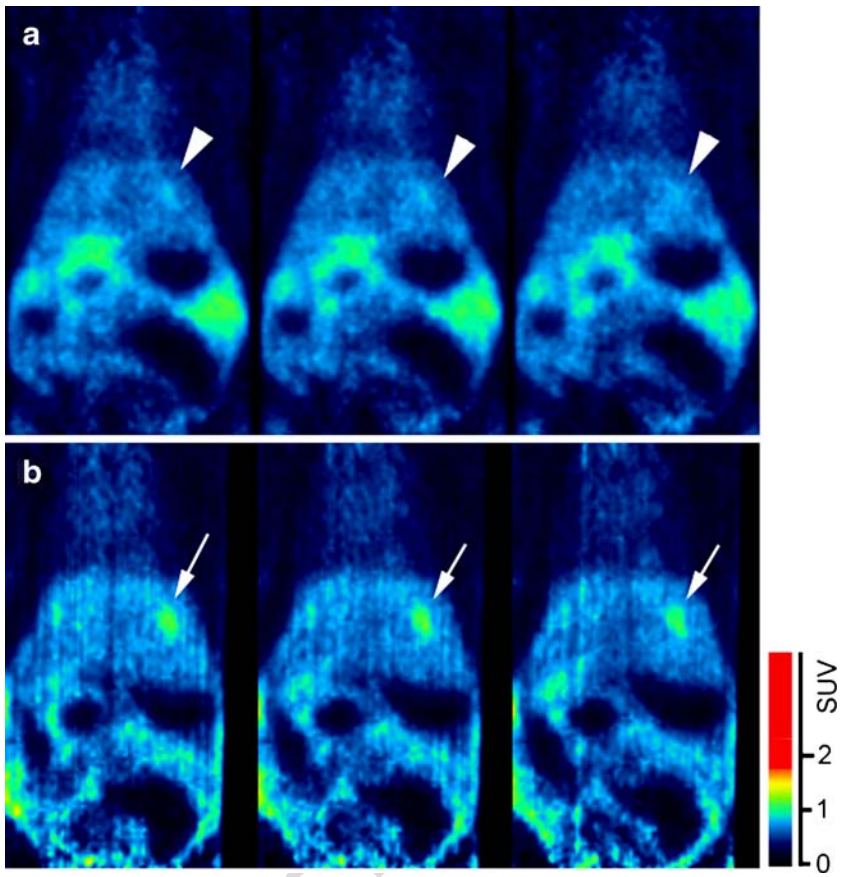

Fig. 2. Coronal views of CCA using C-11 acetate (**a**, *arrow heads*) and FDG (**b**, *arrows*). Image intensity was normalized to liver radioactivity for comparative purposes.

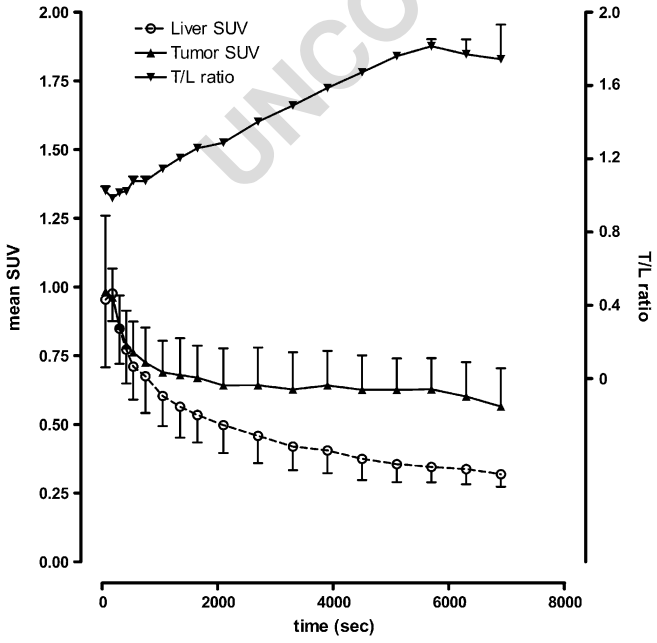

Fig. 3. Time–activity curves of tumor, liver, and T/L ratio in the pilot FDG animal PET study (n=6 rats).

determined as 90 minutes postinjection of the tracer, and FDG was selected as the tracer of choice. A 30-minute period for the static acquisition protocol was used.

Tumor Detection and FDG Uptake

Necropsy and histology confirmed the diagnosis of TAA-induced CCA in 22 out of the 26 experiment rats (84.6%, Table 1). Twenty rats had peripheral mass-forming CCA and two had infiltrative CCA. Static animal PET imaging disclosed FDG-avid hepatic lesions in 17 tumor-bearing rats (77.3%). Two foci of increased FDG uptake were detected in three tumor-bearing rats, whereas three FDG-positive foci were seen in three animals. The average tumor size was 5.3± 2.1 mm in diameter. The sensitivity of animal PET in the detection of CCA was 77% (17/22). There were five rats with false-negative animal PET scans. One case was an infiltrative tumor with heterogeneous FDG uptake throughout the liver (Fig. 4b). The remaining four rats with false–negative animal PET scans had small liver tumors (<2 mm) whose diameters were close to the spatial resolution of the animal PET scanner. No animal developed distant metastases. FDG uptake in nontumoral liver and lung tissues was similar in experiment and control rats. The average values of

JrnlID 11307_ArtID 141_Proof# 1 - 07/04/2008

Q2

t1.1 **Table 1.** True positive, true negative, false positive and false negative of animal PET results, as compared with necropsy, in experiment rats (n=26)

t1.2 Parameter	Necropsy +	Necropsy –	Total
t1.3 Animal PET +	17	0	17
t1.4 Animal PET –	5	4	9
t1.5 Total	22	4	26

the SUV_{mean} and SUV_{max} in nontumoral liver tissue were relatively high in experiment rats, but not significantly different from the control rats. Tumor tissue had higher SUV_{mean} than nontumor tissue, regardless of number of tumors per animal (Table 2). There was a positive correlation between SUV_{mean} and SUV_{max} in both tumor tissue (r^2= 0.74) and in nontumor liver (r^2=0.67) tissue. No correlation was found with the tumor volume.

Correlation Between Ex Vivo Autoradiographic Results and Histological Data

Histopathology revealed invasive intestinal-type CCA with intense stromal desmoplasia. *Ex vivo* autoradiography showed that large tumors, as detected by PET, were actually confluent small tumor nests (Fig. 5). The average tumor size was 2.6±1.5 mm (largest diameter).

The neoplastic glands exhibited prominent intra-luminal necrosis ('comedonecrosis'), an indication of high cellular turnover. In one experiment rat, the liver tumor mass had a large central necrotic area. In this case, animal PET showed intense FDG uptake in the periphery of lesion with no uptake in the center of the liver lesion (doughnut appearance, Fig. 4c). The smallest tumor size that was detected by FDG animal PET was approximately 2 mm (Fig. 5). FDG uptake was not increased in fibrotic areas. The average T/L ratio as determined by quantitative autoradiography was 4.4±0.2 (twofold higher than that calculated with animal PET).

Discussion

The exploitation of novel therapeutic strategies merits a high priority in the treatment of CCA. This highlights the need to carefully investigate the most stringent available preclinical model of this malignancy. We have previously developed an oral TA-induced model of rat CCA that recapitulates the histologic progression of human CCA [11, 22]. In the present study, we sought to evaluate the feasibility of animal PET in detecting CCA in the setting of the TAA rat model.

PET has recently emerged as a valuable imaging modality for the diagnosis and staging of cancer [12]. Until recently, however, PET has not been suitable for small animal models because of resolution limitations. Development of micro-PET instrumentation for small animal imaging has made this technology feasible for the noninvasive, quantitative, and repetitive imaging of biological function in living animals [23]. Our current data show that animal PET in the setting of the TAA rat model is feasible for the detection of CCA.

Both FDG and C-11 acetate have successfully been used as functional probes in tumor imaging. It is worth noting, however, that FDG has emerged as the most reliable tracer in PET imaging of human CCA [24, 25]. In keeping with these observations in humans, we found higher uptake of FDG than C-11 acetate in TTA-induced experimental rat CCA. Interestingly, a higher FDG uptake was found in our model compared with other animal models of hepatocellular carcinoma (HCC) [26]. Altogether, these data suggest a different biological behavior of HCC versus CCA. Notably, FDG-PET has a high average false-negative rate of 40%–50% in the detection of HCC, and the usefulness of C-11 acetate as a radiotracer complementary to FDG in PET imaging of HCC has recently emerged in humans [14, 16].

The incidence of CCA at 20 weeks after initiation of TAA in the present study was similar to that reported previously

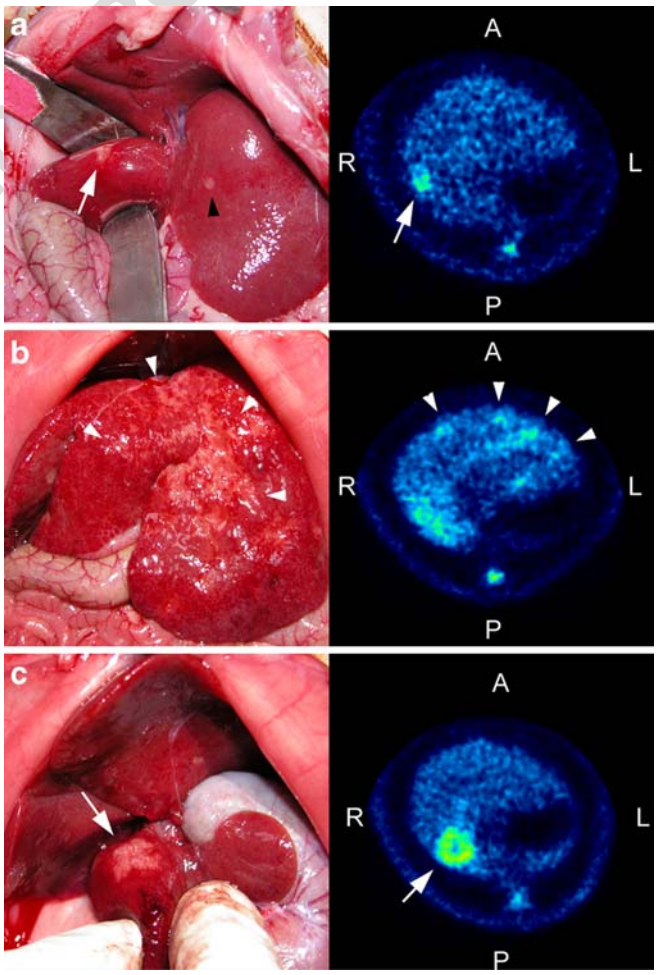

Fig. 4. FDG animal PET images and corresponding necropsy. *White arrows* indicate concordant FDG lesions on both image and necropsy. *Black arrow* heads indicate small tumor nodules not detected by animal PET **a**. Diffuse CCA lesions (**b**) and a doughnut lesion (**c**) were also evident. Image intensity was normalized to liver radioactivity for comparative purposes.

t2.1 **Table 2.** Maximal and mean SUV of nontumor liver tissue and tumor tissue in control and experiment rats

Parameter	Group	Tumor number (subject number)	SUV_{mean}		SUV_{max}		Total tumor volume (cm^3;SD)
			Liver[a] (SD)	Tumor (SD)	Liver[a] (SD)	Tumor (SD)	
Control; rats (n=4)	1	0	0.32		0.56		
		(n=4)	(0.07)		(0.04)		
Experiment; rats (n=26)	2	0	0.37		0.61		
		(n=9)	(0.08)		(0.12)		
	3	1	0.39	0.61[b]	0.64	0.81[b]	0.05
		(n=11)	(0.08)	(0.12)	(0.10)	(0.14)	(0.03)
	4	2	0.42	0.76[b]	0.68	1.07[b]	0.27
		(n=3)	(0.05)	(0.11)	(0.14)	(0.19)	(0.20)
	5	3	0.38	0.62[b]	0.57	0.84[b]	0.38
		(n=3)	(0.11)	(0.13)	(0.16)	(0.22)	(0.27)

t2.14 Animals were divided into five groups according to the number of tumors detected by animal PET
SUV Standardized uptake value, *SD* standard deviation
[a]Liver SUV_{mean} and SUV_{max} were compared across group 1~5 (SUV_{mean}, p=0.478; SUV_{max}, p=0.409, Kruskal–Wallis test)
[b]SUV_{mean} and SUV_{max} were compared in tumor and nontumor liver tissue in groups 3~5 (all p<0.05, the only exception being comparison of SUV_{max} in group 5 (p=0.116). Mann–Whitney U test)

[11]. However, detection rates of CCA were lower for animal PET compared with necropsy. Several possible explanations could be considered to account for these findings. Firstly, animal PET with FDG may fail to show enhanced accumulation in tumor tissue, as previously reported in human PET studies [27]. Second, although accuracy in detecting tumors larger than 2 mm is high, animal PET may miss approximately 35% of tumors smaller than 1 mm [28]. According to our autoradiography results, our animal PET scanner cannot detect CCA that are less than 2 mm in size. The presence of such small tumors may cause a high liver background in the experiment rats compared to the control group.

As can be seen in Fig. 4b, infiltrative CCA in the TAA rat model often is not easily distinguished from normal liver background due to the lack of distinct borders. Similar findings have been recently reported in humans [29]. Under these circumstances, the only abnormal finding on PET may be a relative increase in FDG uptake in the liver parenchyma. This shortcoming of PET has encouraged the development of the tumor viability index (TVI) to quantitatively measure tumor growth instead of using the SUV of the tumor tissue [30]. TVI values are calculated by subtracting FDG uptake in the normal liver tissue from the FDG uptake in the whole liver region (including tumor nodules). A major drawback of this index is that the selection of a normal liver region and the placement of the ROIs for the whole liver may be not easily defined in animal PET studies.

Given the lack of adequate software support, attenuation correction was not applied in our study. Although less prominent in animal PET than in humans, attenuation correction may influence lesion detectability. In this regard, a previous study has shown that attenuation correction can improve resolution by 0.2 mm in animal PET imaging [31]. Our current data also show that the average T/L ratio as determined by quantitative autoradiography was twofold higher than that calculated with attenuated animal PET. In addition, partial volume correction (PVC) may improve detection of small tumors and allow accurate quantitation of tracer. Moreover, an iterative postreconstruction PVC correction may generate more accurate uptake measurements in subcentimeter tumors than the uncorrected values [32]. Although fine correction methods were not applied in our

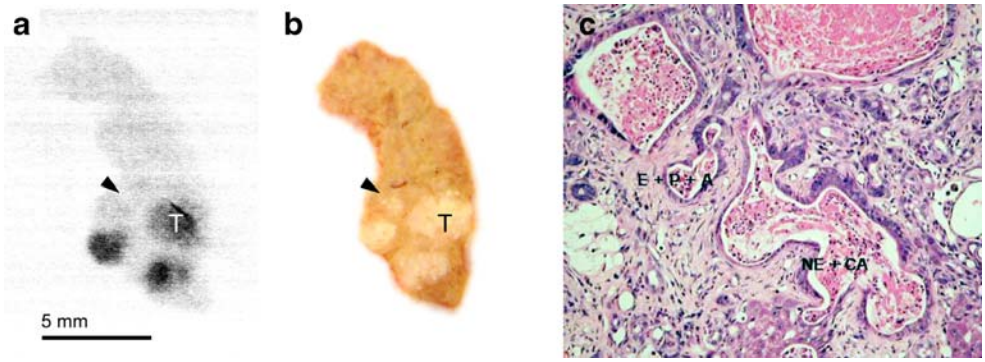

Fig. 5. Autoradiography (**a**), necropsy (**b**) and histology (**c**) findings showing confluent tumors (approximately 2 mm in size). Some CCA lesions failed to accumulate FDG (*arrow head*). *E* Enlargement, *P* proliferation, *A* atypia, *NE* comedonecrosis, *CA* carcinoma.

study, the sensitivity and specificity of animal PET in the detection of CCA were 77% (17/22) and 100% (4/4), respectively. The use of a robust animal model such as the TAA rat model may account for such diagnostic accuracy of animal PET.

The T/L ratio in our pilot dynamic studies was relatively low compared to human studies [24, 29]. The T/L ratio, however, was not uniformly distributed throughout different tumor sizes (Fig. 4a and c), and partial volume effects may not be negligible in small animal studies. Furthermore, the radioactivity time course after exposure may be different in human and animal studies [33]. It is also possible that TTA-induced CCAs might have different glucose-regulating mechanisms from those of human cholangiocarcinomas [24].

In general, we have shown a good positive correlation between SUV_{max} and SUV_{mean}, the only exception being large tumors with areas of central necrosis. These necrotic areas contain a highly heterogeneous distribution of FDG uptake. Moreover, SUV_{max} and SUV_{mean} did not correlate significantly with tumor volume. As can be seen in Table 2, similar SUV values were observed across different study groups. Accordingly, SUV_{max}, SUV_{mean}, and tumor volume should all be taken into account when evaluating tumor response to therapy. In this regard, total lesion glycolysis has been proposed as an objective measurement of clinical treatment response [34].

FDG accumulated in both tumor and infectious lesions [35]. As liver inflammation may occur after ingestion of the toxin, tumor detectability in the TTA rat model might be diminished by the presence of TAA-induced centrilobular liver inflammation [36]. Due to different FDG uptake kinetics between inflammatory and tumoral foci, it might be useful to distinguish these two entities by scanning the subject at a later time period [37]. In our study, the use of an optimal scan time (90 minutes postinjection of the FDG) resulted in no FDG accumulation in cirrhotic lesions.

A previous clinical study has shown that FDG-PET may be of value in discovering unsuspected distant metastases in patients with CCA [24]. In our study, no extrahepatic metastases were detected by either animal PET or necropsy. It is worth noting, however, that it is unlikely that metastatic lesions may develop during the early course of CCA.

Conclusions

In conclusion, this study demonstrates that animal PET in the setting of the TAA rat model seems to be feasible for the detection of CCA. Future translational studies are needed to confirm and expand our findings.

Acknowledgments. This study was supported by grants from the Chang Gung Medical Research Program (Grants # 33103 and 340192) and the National Medical Research Program (Grant # 340551).

References

1. de Groen PC, Gores GJ, LaRusso NF, Gunderson LL, Nagorney DM (1999) Biliary tract cancers. N Engl J Med 341:1368–1378
2. Ahrendt SA, Nakeeb A, Pitt HA (2001) Cholangiocarcinoma. Clin Liver Dis 5:191–218
3. bores-Saavedra J, Henson DE, Sobin LH (1992) The WHO histological classification of tumors of the gallbladder and extrahepatic bile ducts. A commentary on the second edition. Cancer 70:410–414
4. Fleming KA, Boberg KM, Glaumann H et al (2001) Biliary dysplasia as a marker of cholangiocarcinoma in primary sclerosing cholangitis. J Hepatol 34:360–365
5. Hansel DE, Rahman A, Hidalgo M et al (2003) Identification of novel cellular targets in biliary tract cancers using global gene expression technology. Am J Pathol 163:217–229
6. Terada T, Nakanuma Y, Sirica AE (1998) Immunohistochemical demonstration of MET overexpression in human intrahepatic cholangiocarcinoma and in hepatolithiasis. Hum Pathol 29:175–180
7. Endo K, Yoon BI, Pairojkul C, Demetris AJ, Sirica AE (2002) ERBB-2 overexpression and cyclooxygenase-2 up–regulation in human cholangiocarcinoma and risk conditions. Hepatology 36:439–450
8. Villa R, Gornati D, Zaffaroni N et al (1997) Comparative *in vitro* sensitivity of human cholangiocarcinoma and colon adenocarcinoma cells to anticancer agents. Anticancer Res 17:961–968
9. Hudd C, Euhus DM, LaRegina MC et al (1985) Effect of cholecystokinin on human cholangiocarcinoma xenografted into nude mice. Cancer Res 45:1372–1377
10. Sirica AE (2005) Cholangiocarcinoma: molecular targeting strategies for chemoprevention and therapy. Hepatology 41:5–15
11. Yeh CN, Maitra A, Lee KF, Jan YY, Chen MF (2004) Thioacetamide-induced intestinal-type cholangiocarcinoma in rat: an animal model recapitulating the multi-stage progression of human cholangiocarcinoma. Carcinogenesis 25:631–636
12. Kelloff GJ, Hoffman JM, Johnson B et al (2005) Progress and promise of FDG-PET imaging for cancer patient management and oncologic drug development. Clin Cancer Res 11:2785–2808
13. Keiding S, Hansen SB, Rasmussen HH et al (1998) Detection of cholangiocarcinoma in primary sclerosing cholangitis by positron emission tomography. Hepatology 28:700–706
14. Ho CL, Yu SC, Yeung DW (2003) 11C-acetate PET imaging in hepatocellular carcinoma and other liver masses. J Nucl Med 44: 213–221
15. Oyama N, Akino H, Kanamaru H et al (2002) 11C-acetate PET imaging of prostate cancer. J Nucl Med 43:181–186
16. Ho CL, Chen S, Yeung DW, Cheng TK (2007) Dual-tracer PET/CT imaging in evaluation of metastatic hepatocellular carcinoma. J Nucl Med 48:902–909
17. Laverman P, Blokx WA, Te Morsche RH et al (2007) [(18)F]FDG accumulation in an experimental model of multistage progression of cholangiocarcinoma. Hepatol Res 37:127–132
18. Ishiwata K, Ishii S, Senda M (2005) Successive preparation of C-11 labeled sodium acetate and/or sodium hexanoate. Appl Radiat Isot 46:1035–1037
19. Fuchtner F, Steinbach J, Mading P, Johannsen B (1996) Basic hydrolysis of 2-[F-18]fluoro-1,3,4,6-tetra-*O*-acetyl-D-glucose in the preparation of 2-[F-18]fluoro-2-dexoy-D-glucose. Appl Radiat Isot 47:61–66
20. Lin KJ, Yen TC, Wey SP et al (2004) Characterization of the binding sites for 123I-ADAM and the relationship to the serotonin transporter in rat and mouse brains using quantitative autoradiography. J Nucl Med 45:673–681
21. Young H, Baum R, Cremerius U et al (1999) Measurement of clinical and subclinical tumour response using [18F]-fluorodeoxyglucose and positron emission tomography: review and 1999 EORTC recommendations. European Organization for Research and Treatment of Cancer (EORTC) PET Study Group. Eur J Cancer 35:1773–1782
22. Jan YY, Yeh TS, Yeh JN, Yang HR, Chen MF (2004) Expression of epidermal growth factor receptor, apomucins, matrix metalloproteinases, and p53 in rat and human cholangiocarcinoma: appraisal of an animal model of cholangiocarcinoma. Ann Surg 240:89–94
23. Cherry SR, Gambhir SS (2001) Use of positron emission tomography in animal research. ILAR J 42:219–232
24. Kim YJ, Yun M, Lee WJ, Kim KS, Lee JD (2003) Usefulness of 18F-FDG PET in intrahepatic cholangiocarcinoma. Eur J Nucl Med Mol Imaging 30:1467–1472
25. Fritscher-Ravens A, Bohuslavizki KH, Broering DC et al (2001) FDG PET in the diagnosis of hilar cholangiocarcinoma. Nucl Med Commun 22:1277–1285

26. Salem N, MacLennan GT, Kuang Y et al (2007) Quantitative evaluation of 2-deoxy-2[F-18]fluoro-D-glucose-positron emission tomography imaging on the woodchuck model of hepatocellular carcinoma with histological correlation. Mol Imaging Biol 9:135–143
27. Lee JD, Yang WI, Park YN et al (2005) Different glucose uptake and glycolytic mechanisms between hepatocellular carcinoma and intrahepatic mass–forming cholangiocarcinoma with increased (18)F–FDG uptake. J Nucl Med 46:1753–1759
28. Kondo S, Hosono MN, Wada Y et al (2004) Use of FDG–microPET for detection of small nodules in a rabbit model of pulmonary metastatic cancer. Ann Nucl Med 18:51–57
29. Jadvar H, Henderson RW, Conti PS (2007) [F-18]fluorodeoxyglucose positron emission tomography and positron emission tomography: computed tomography in recurrent and metastatic cholangiocarcinoma. J Comput Assist Tomogr 31:223–228
30. Ishiwata K, Liu HY, Teramoto K et al (2006) Tumor viability evaluation by positron emission tomography with [18F]FDG in the liver metastasis rat model. Ann Nucl Med 20:463–469
31. Yao R, Seidel J, Johnson CA et al (2000) Performance characteristics of the 3-D OSEM algorithm in the reconstruction of small animal PET images. Ordered-subsets expectation-maximization. IEEE Trans Med Imaging 19:798–804
32. Teo BK, Seo Y, Bacharach SL et al (2007) Partial-volume correction in pet: validation of an iterative postreconstruction method with phantom and patient data. J Nucl Med 48:802–810
33. Keiding S, Munk OL, Schiott KM, Hansen SB (2000) Dynamic 2-[18F] fluoro-2-deoxy-D–glucose positron emission tomography of liver tumours without blood sampling. Eur J Nucl Med 27:407–412
34. Hong D, Lunagomez S, Kim EE et al (2005) Value of baseline positron emission tomography for predicting overall survival in patient with nonmetastatic esophageal or gastroesophageal junction carcinoma. Cancer 104:1620–1626
35. Stumpe KD, Dazzi H, Schaffner A, von Schulthess GK (2000) Infection imaging using whole–body FDG–PET. Eur J Nucl Med 27:822–832
36. Tietge UJ, Selberg O, Kreter A et al (2004) Alterations in glucose metabolism associated with liver cirrhosis persist in the clinically stable long-term course after liver transplantation. Liver Transpl 10:1030–1040
37. Hamazawa Y, Koyama K, Okamura T et al (2007) Comparison of dynamic FDG–microPET study in a rabbit turpentine–induced inflammatory model and in a rabbit VX2 tumor model. Ann Nucl Med 21:47–55